Nonlinear modification of the stability of fast particle driven modes in tokamaks

Nonlinear modification of the stability of fast particle driven modes in tokamaks

C Nguyen[1], X Garbet[2], V Grandgirard[2], J Decker[2], Z Guimarães-Filho[3], M Lesur[4], H Lütjens[1], A Merle[2] and R Sabot[2]

[1] Centre de Physique Théorique, CNRS-Ecole Polytechnique, Palaiseau, France
[2] CEA, IRFM, F-13108 Saint-Paul-lez-Durance, France
[3] PIIM, Université de Provence, F-13397 Marseille, France
[4] JAEA, Higashi-Ueno 6-9-3, Taitou, Tokyo, 110-0015, Japan

E-mail: christine.nguyen@cpht.polytechnique.fr

Abstract

In the nonlinear regime, the stability of resonantly driven systems, such as energetic particle driven modes in magnetically confined plasmas, is shown to depend on the presence and nature of an underlying damping mechanism. When resonant damping is involved, subcritical states can occur. In particular, purely nonlinear steady-state regimes can be postulated, whose destabilization threshold and saturation levels are calculated and validated using a reduced one-dimensional paradigmatic bump-on-tail model. The applicability of the developed model to realistic tokamak acoustic modes is assessed. It is shown that purely nonlinear steady-state regimes are possible under standard tokamak conditions.

(Some figures in this article are in colour only in the electronic version)

1. Introduction

In fusion devices, suprathermal particles with energies of the order of 100 keV to a few MeV are well known to drive magnetohydrodynamic (MHD) like modes in the thermonuclear plasma, via resonant excitation [1]. Such a dynamics has been observed in the Tore-Supra tokamak for the so-called fast electron driven fishbone modes [2, 3] and fast ion driven Beta Alfvén eigenmodes [4, 5].

In order to understand and control the latter modes which can have deleterious effects on the plasma confinement, various theoretical and experimental stability analysis have been conducted [6, 7], which are mainly based on linear considerations. More recently, several nonlinear models have also been developed and shown to describe various experimental behaviours successfully [8, 9]. Several reasons justify the use of purely nonlinear descriptions

for both the mode structure [10, 11] and the driving energetic particles [12, 13]. First, since resonant physics involves fast time scales, the nonlinear regime can be expected to be reached rapidly, even for relatively low linear growth rates. Secondly, some experimental conditions have been estimated to be much above the mode destabilization threshold, which favours the emergence of strong growth rates [13]. Next, the fine structures of the modes involved can favour the emergence of strong mode–mode coupling. And finally, fusion plasmas are characterized by temporarily abrupt events such as sawtooth crashes which can temporarily move the thermonuclear plasma away from equilibrium and hence make possible the access to purely nonlinear states.

This paper questions the possibility of a nonlinear modification of stability, or more precisely, the existence of purely nonlinear modes which can live, once excited, because damping shrinks nonlinearly. Two ideas of this study are believed to deserve investigation: the modification of stability thresholds related to nonlinear physics, and the consideration of a self-consistent damping, somehow overlooked in earlier kinetic studies (past models usually consider a fixed damping rate [9, 12, 14]). In this paper, the focus is on kinetic resonant nonlinearities: energetic particle induced resonant drive is computed along with resonant damping of the Landau type. More generally, we believe that the simultaneous calculation of energetic resonant drive and self-consistent background damping, e.g. continuum damping for Alfvén waves, can bring interesting and relevant behaviours. The present kinetic model involving both resonant damping and drive, applies to tokamak acoustic modes, such as beta Alfvén eigenmodes and geodesic acoustic modes [15]. In tokamaks, linear stability studies of the latter waves have been performed in JET [16] and Tore-Supra [17], which confirm that they are resonantly driven by fast ions and damped by thermal ion Landau damping.

In the following, a reduced model is used which is paradigmatic for the kinetic dynamics of the modes quoted above. It shows that a subcritical activity can take place and in particular *metastable modes*, defined here as subcritical steady-state saturated modes. This paper complements the submitted letter [18] and provides application to real tokamak conditions. In section 2, the model used in this analysis is described and the outcome of its numerical implementation compared with earlier simulations of a similar type [19, 20]. In section 3, the possibility for metastable modes to take place is analyzed analytically. A metastable stability threshold is derived as well as the expected saturation levels of the latter modes. Next, the results are compared with simulations. Finally, in section 4, the model developed in the paper is applied to real tokamak conditions and its relevance discussed.

2. Model

2.1. Model description

The nonlinear evolution of resonant mechanisms has been widely studied using adapted versions of the one-dimensional electrostatic bump-on-tail problem [14, 21]. The latter problem is recognized to describe the kinetic (resonance related) nonlinear features of fast particle driven modes appropriately. In its most studied version which includes a fixed and constant background damping rate, it has been shown to describe a variety of experimental behaviours characterizing toroidal Alfvén eigenmodes or Fishbone modes [9, 8, 22].

Similarly, in this study, we make use of a 1D multi-species electrostatic bump-on-tail model. More precisely, the traditional Vlasov–Poisson system describing the resonant excitation of Langmuir waves by electrons in a fixed background of ions [23] is used in its collisional version, and completed with one additional collisional Vlasov equation, intended to induce a tunable and self-consistent resonant damping. More precisely, two Vlasov equations

2

with collisions are combined with Poisson equation

$$\partial_t F_i + v \partial_x F_i + \frac{e_i E}{m_i} \partial_v F_i = -\nu_i [F_i - F_{i\,\mathrm{eq}}(v)], \qquad i = 1, 2, \tag{1}$$

$$-\partial_x E = \sum_{i=1,2} e_i \int \mathrm{d}v [F_i - F_{i\,\mathrm{eq}}(v)]. \tag{2}$$

Additionally, the above equations have been normalized for simplicity and numerical implementation, using arbitrary reference quantities for the density, temperature, charge and mass n, T, e, m, and normalizing frequencies by $\omega_p = \sqrt{ne^2/m\epsilon_0}$ with ϵ_0 the dielectric constant in vacuum, lengths by $\lambda = \sqrt{\epsilon_0 T/ne^2}$, velocities by $v_t = \sqrt{T/m}$, distribution functions by v_t/n, the electric field by $\sqrt{\epsilon/nT}$ and finally charges and masses, respectively by e and m.

Moreover, equilibrium distribution functions are taken to be of the form

$$F_{1\,\mathrm{eq}} = \frac{n_b}{\sqrt{2\pi}\,v_{tb}} \exp\left[-\frac{1}{2}\left(\frac{v}{v_{tb}}\right)^2\right] + \frac{n_e}{\sqrt{2\pi}\,v_{te}} \exp\left[-\frac{1}{2}\left(\frac{v-v_0}{v_{te}}\right)^2\right], \tag{3}$$

$$F_{2\,\mathrm{eq}} = \frac{n_d}{\sqrt{2\pi}\,v_{td}} \exp\left[-\frac{1}{2}\left(\frac{v}{v_{td}}\right)^2\right]. \tag{4}$$

where n_s and v_{ts} (for $s =$ b, e, d), respectively, represent the density and thermal velocity of the species s, where s belongs to one of the three categories: the *bulk*, the *exciting* species or the *damping* species. $F_{1\,\mathrm{eq}}$ is indeed divided into a thermal *bulk*, and a bump on tail, designed to provide resonant *excitation*. Hence, in the absence of the second species, the present model is equivalent to the collisional bump-on-tail model developed in [14, 21], except for the collisionality which is here simply taken to be constant and unique for the bulk and the bump: $\nu_b = \nu_e = \nu_1$. A second evolving species with a thermal distribution and a collisionality $\nu_d = \nu_2$ is now added to include a tunable resonant *damping*.

Finally, the system is perturbed using a distribution function at time $t = 0$,

$$F_1(x, v, t = 0) = F_{1\mathrm{eq}}[1 + \alpha \cos(kx)]. \tag{5}$$

The model has been implemented numerically using a semi-Lagrangian method, developed in the framework of the multi-scheme CALVI platform [24].

2.2. Investigated limit

The aim of this paper being to demonstrate the possibility of a nonlinear modification of stability, the following limit is used: (i) cold-bulk: $\omega_{pb} \equiv \sqrt{n_b e_b^2/m_b} \gg k v_b$ where ω_{pb} is the bulk plasma frequency; (ii) perturbative: $n_b \gg n_e, n_d$ and $\omega_{pb} \gg \nu_b, \nu_e, \nu_d$; (iii) monochromatic (verified *a posteriori*): $\omega_{Bs} \gg \omega_{pb}(v_0/v_{ts})$, with $\omega_{Bs} = \sqrt{|e_s|Ek/m_s}$ a measure of the perturbation amplitude whose physical interpretation will be clarified below. This allows us to take dissipation and drive only at the first order, and to assume dissipation to result mainly from collisions.

Accordingly, the simulations displayed below make use of the fixed parameters $e_s = 1.0$ for $s =$ b, e, d, $m_s = 1.0$ for $s =$ b, e, $n_b = 1.0$, $v_{tb} = 0.3$, $n_e = 0.03$, $v_{te} = 1.0$ $v_0 = 4.5$, $v_{td} = 2.5$ and $k = 0.3$. The remaining ones (n_d, m_d/m_e and the collisionalities ν_e and ν_d) are the variable parameters of our analysis. In particular, collisionalities are chosen independently of the other parameters, since the model is intended to be paradigmatic and to cover various types of dissipative effects.
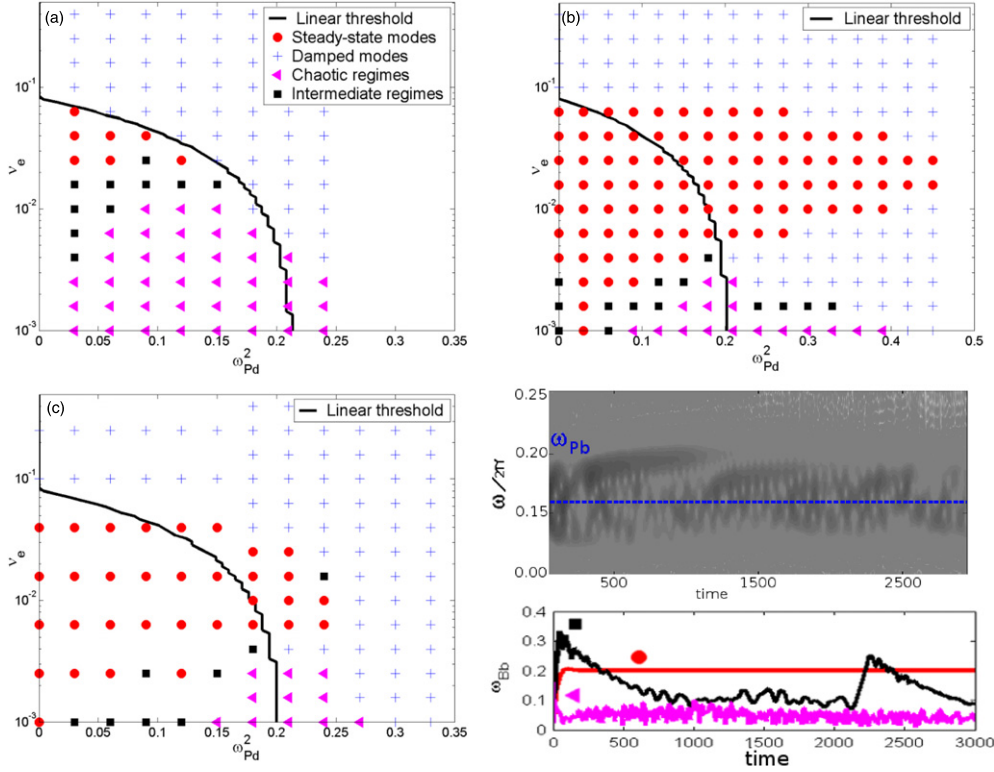
Figure 1. Diagram of nonlinear states obtained for (*a*) $m_d/m_l = 2.0$, $\nu_d = 0.04$, $\omega_{Bb}(0) = 0.2$; (*b*) $m_d/m_l = 0.5$, $\nu_d = 0.005$, $\omega_{Bb}(0) = 0.2$; (*c*) $m_d/m_l = 0.5$, $\nu_d = 0.04$, $\omega_{Bb}(0) = 0.05$. The distinguished states are illustrated in the lower-right hand corner, where an example of chaotic behaviour is shown in a spectrogram of the mode amplitude, along with the time evolution of the mode amplitudes for different types of behaviours.

2.3. Outcome and comparison with previous work

In figure 1, simulation results corresponding to three sets of parameters are displayed and put in the same form as in [19, 20] for comparison: simulated nonlinear states are reported in the (ω_{pd}^2, ν_e) plane for fixed values of the initial perturbation, of m_d/m_l and of ν_d. Four types of behaviours are distinguished. Modes with a vanishing amplitude are referred to as *damped*, modes with a single frequency and constant amplitude as *steady-state and saturated* and oscillations characterized by a large frequency spectrum as *chaotic*. Finally, behaviours which do not clearly enter one of these categories have simply been reported as *intermediate*, and include for example periodic and excitation-relaxation dynamics [12, 25]. Moreover, the linear stability threshold is indicated, and derived from the numerical resolution of equation (6),

$$-k^2 = \sum_{s=b,e,d} \frac{\omega_{ps}^2}{v_{ts}^2} Y\left(\frac{\omega + i\nu_s - \delta_{se}kv_0}{\sqrt{2}kv_{ts}}\right), \qquad (6)$$

(where $Y(x) = (1 + x)Z(x)$ and Z the plasma dispersion function), which is directly seen to be the linear dispersion relation corresponding to equations (1) and (2).

It can directly be noted that the various diagrams of figure 1 reproduce a similar distribution of nonlinear states as the more traditional bump-on-tail model with a fixed damping rate [19, 20]. The new feature here comes from the comparison with the linear stability threshold,

which obviously does not explain all the occurrences of modes. In agreement with the other simulated parameters (see below), we note that (i) in any case, the perturbation survives inside the linear unstable region; (ii) a subcritical activity is present which concerns both chaotic and steady-state saturated modes. Moreover, in the case of higher v_d and higher m_d, subcritical steady-state modes disappear, but cases with a complete cancellation of subcritical chaotic modes have not been found; (iii) when the initial perturbation amplitude is reduced keeping other parameters fixed, subcritical activity shrinks.

Subcritical chaotic modes are reminiscent of some observations performed in the case of a fixed damping rate [21, 20], and are out of the scope of this paper. In the following, we focus on steady-state saturated modes, called here *metastable* states.

3. Analysis of metastable modes

In this section, we suggest an explanation for the presence of metastable modes, and provide the corresponding destabilization threshold and nonlinear saturation level.

3.1. Necessary condition for steady-state saturation

In the limit investigated here, the linear dispersion relation, equation (6), can be treated perturbatively, taking excitation and damping at the first order only. It is well known that the leading order returns an oscillation of absolute frequency $|\omega_{pb}|$. Then, equation (6) taken at the first order directly shows that the bump and damping species, respectively, provide independent *exciting* and *damping* rates γ_e and $-\gamma_d$ ($\gamma_d > 0$) with

$$\gamma_s = \left| 0.5 \frac{\omega_{pb}}{k^2} \frac{\omega_{ps}^2}{v_{ts}^2} \text{ Im } Y \left(\frac{\omega_{pb} - \delta_{se} k v_0}{\sqrt{2} k v_{ts}} \right) \right| \qquad \text{for } s = \text{e, d,} \qquad (7)$$

such that the mode growth rate can be approximated by $\gamma_L \approx \gamma_e - \gamma_d - v_b$.

In the nonlinear regime, the traditional bump-on-tail model with a fixed damping rate γ_d is known to enable steady-state saturation inside the linear unstable region [14]. Saturation is due to the reduction of resonant drive. In particular, when the bouncing frequency of driving resonant particles inside the mode verifies $\omega_{Be} \equiv \sqrt{|e_e|Ek/m_e} \gg v_e, \omega(v_0/v_{te})$ (E the magnitude of the perturbed electric field), decorrelation processes are weak and resonant particles are deeply trapped inside the wave. In this case, it is shown in [14] that resonant drive is reduced by the factor $cv_e^* \equiv c(v_e/\omega_{Be})$ with $c \approx 2.0$. Hence, saturation is possible for $cv_e^* \gamma_e = \gamma_d + v_b$.

When now a self-consistent damping is taken into account, the perturbative limit makes possible the independent treatment of the exciting and damping species. Since the calculation of [14] does not depend on the sign of the resonant energy transfer, but simply on the presence of a wave–particle resonance, it applies to damping as well. Consequently, damping can be expected to be nonlinearly reduced to $-cv_d^* \gamma_d \equiv -c(v_d/\omega_{Bd})\gamma_d$ (where again $\omega_{Bd} = \sqrt{|e_d|Ek/m_d}$).

Moreover, in order to avoid the condition of deep trapping $\omega_{Bs} \gg v_s$ for ($s = \text{e, d}$) and hence, to make possible a complete investigation of the stability diagrams, we make use of modified reduction factors $cv_s^*/(1 + cv_s^*)$, which clearly return the above result in the regime of deep trapping ($v_s^* \ll 1$). When v_s^* becomes large $cv_s^*/(1+cv_s^*)$ goes to 1 which matches the idea that the linear regime is conserved when nonlinear trapping is ineffective compared with equilibrium restoring mechanisms, as in the traditional collisional plateau regime. Following

5
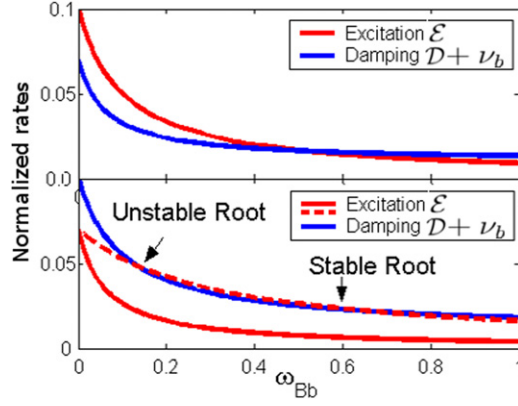
Figure 2. Schematic of the different possible relative positions of the nonlinear damping and driving curves as a function of the mode amplitude. Intersections correspond to possible steady-state saturation levels.

these remarks, the condition for saturation reads as

$$\mathcal{E}(\omega_{Bb}) = \mathcal{D}(\omega_{Bb}) + \nu_b \qquad \text{with} \quad \begin{cases} \mathcal{E}(\omega_{Bb}) \equiv \dfrac{c\nu_e}{\omega_{Be} + c\nu_e}\gamma_e, \\[2mm] \mathcal{D}(\omega_{Bb}) \equiv \dfrac{c\nu_d}{\omega_{Bd} + c\nu_d}\gamma_d, \end{cases} \tag{8}$$

and steady-state modes are possible if this equation has positive solutions for the mode amplitude, written here in terms of ω_{Bb} ($\propto \sqrt{E}$).

Equation (8) is a second order equation. When $\gamma_L \equiv \gamma_e - \gamma_d - \nu_b > 0$, that is in the linear unstable region, it always has a positive solution. In the subcritical region, positive solutions exist if

$$\gamma_{NL} \equiv \nu_e^*(\gamma_e - \nu_b) - \nu_d^*(\gamma_d + \nu_b) > 0, \tag{9}$$

and

$$\Delta \equiv (\gamma_{NL})^2 - 4\nu_e^*\nu_d^*\nu_b|\gamma_L| > 0 \tag{10}$$

(note that the notation ν_s^* is used here for readability, although the two inequalities do certainly not depend on the mode amplitude). More precisely, in the subcritical case, equation (8) has two positive solutions

$$\omega_{Bb}^{\pm} = (\bar{\gamma}_{NL} \pm \sqrt{\bar{\Delta}})/2\nu_b \qquad \text{where } \bar{\gamma}_{NL} \equiv \gamma_{NL}/\omega_{Bb} \text{ and } \bar{\Delta} \equiv \Delta/\omega_{Bb}^2. \tag{11}$$

The solutions are schematically shown in figure 2. As illustrated in this figure, it is easy to see that in the subcritical case, $\mathcal{E}' - \mathcal{D}'$ is positive for the lower solution and negative for the upper one. Hence, only the higher solution ω_{Bb}^+ is stable, and the corresponding saturation amplitude is shown in figure 3. Interestingly, it can be noted that the existence of solutions in the whole linear stable region is a result of our choices for the determination of saturation. Simply considering the deep trapping limit for the nonlinear reduction factors and neglecting the bulk dissipation in equation (8) leads to a degenerate equation from which saturation amplitudes cannot be obtained. Inclusion of ν_b in equation (8) returns positive solutions in regions A and B of figure 3, whereas the inclusion of a modified return positive solutions in regions B and C only.

6
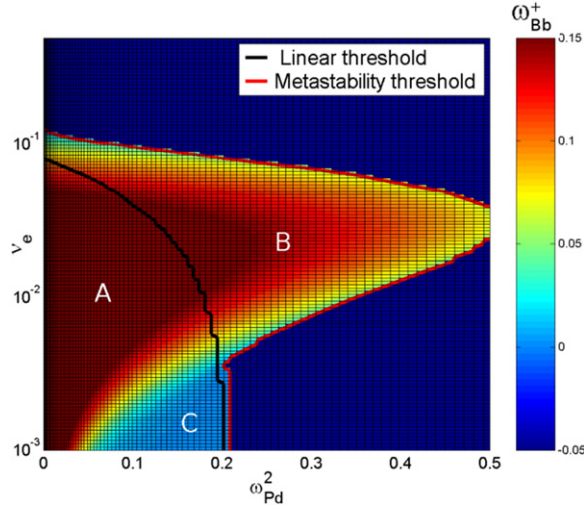
Figure 3. Upper positive solution, equation (8). Note that negative values have been used to represent the absence of positive solutions.

3.2. Numerical validation

To check the relevance of equations (9), (10) and (11), (ω_{pd}^2, ν_e) diagrams have been simulated for the parameters: $m_d/m_e = 0.5, 1.0$, $\nu_d = 0.001, 0.005, 0.01$ with various amplitudes for the initial perturbation: $\omega_{Bb}(0) = 0.2, 0.1, 0.05, 0.025$. Three examples are shown in figure 4 where the initial perturbation amplitude ($\omega_B(0) = 0.2$) has been chosen to be large enough to avoid strong modification of the diagram for larger $\omega_B(0)$. The nonlinear destabilization threshold derived from equations (9) and (10) is shown in these figures, and is found to appropriately describe the emergence of metastable modes. In the fourth picture of equation (4), the saturation levels of simulated steady-state modes are compared with equation (11) both in the linearly stable and unstable regions. Again, a good agreement is found, which confirms in particular that the saturation is independent of the initial pertubation. In this figure, the systematic undershoot of the model compared with simulations may be due to the breaking of the assumption of monochromaticity, that is, the presence of a reduced noise with different wave numbers in the simulations.

3.3. Triggering condition

Finally, we could determine in equations (9) and (10) the limit of the parametric region where metastable modes can take place. Nevertheless, such a condition is not sufficient and the calculation assumes in particular that the nonlinear regime is reached, which may not be the case depending on the initial perturbation. Hence the vanishing of modes with lower initial perturbation shown in figure 1.

In figure 5, the onset of subcritical activity is compared with three criteria:

- The necessity to access the nonlinear regime: since the onset of metastability is a consequence of the damping nonlinear drop, it makes sense to require sufficient time for a modification of the damping species distribution function before the mode gets linearly
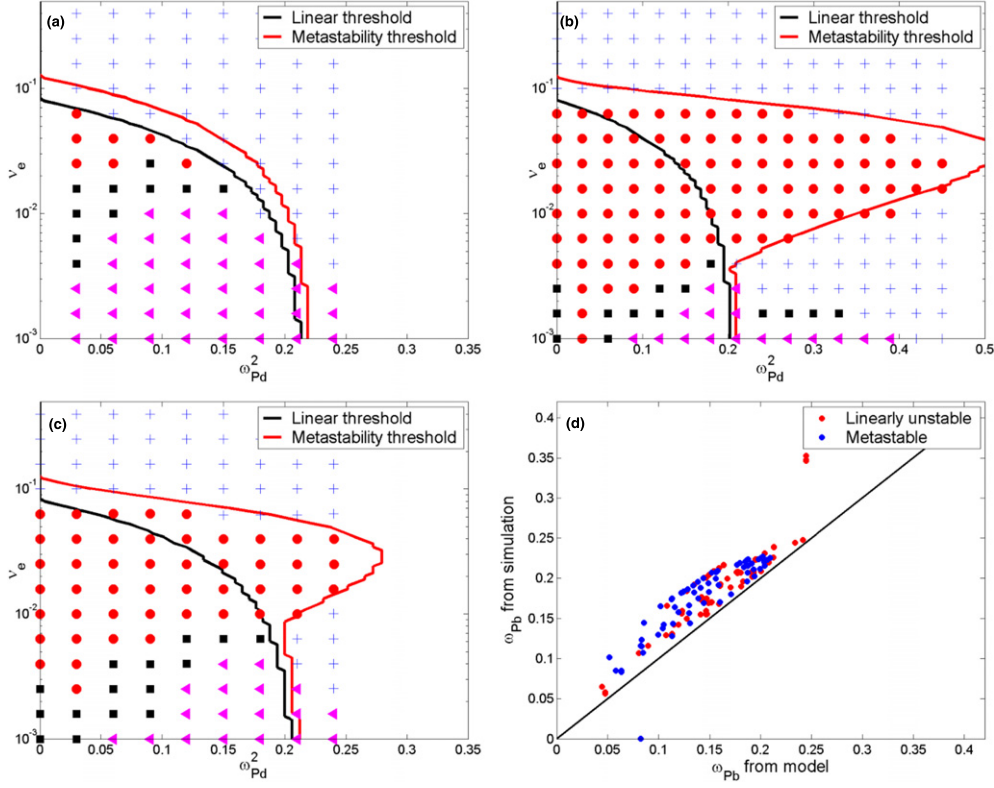
Figure 4. Diagrams of nonlinear states compared with prediction, for (*a*) $m_d/m_l = 2.0$, $\nu_d = 0.04$, $\omega_{Bb}(0) = 0.2$; (*b*) $m_d/m_l = 0.5$, $\nu_d = 0.005$, $\omega_{Bb}(0) = 0.2$; (*c*) $m_d/m_l = 0.5$, $\nu_d = 0.01$, $\omega_{Bb}(0) = 0.2$. In figure (*d*), simulated steady-state saturation levels compared with prediction, for $m_d/m_l \in \{0.5, 2.0\}$, $\nu_d \in \{0.001, 0.005, 0.01\}$, and full scans in $\nu_b \in [10^{-3}, 0.1]$, $\omega_{pd}^2 \in [0.0, 0.35]$.

damped, or

$$\omega_{Bd}(0) = \sqrt{\frac{|e_d|}{|e_b|}\frac{m_b}{m_d}}\,\omega_{Bb}(0) \geqslant -\gamma_L. \tag{12}$$

- The condition for the metastable solution to be an attracting point: even when the nonlinear regime is reached, it is obvious from figure 2 that the solution ω_{Bb}^+ is attractive, in the metastable region, only for a magnitude:

$$\omega_{Bb}(0) \geqslant \omega_{Bb}^-. \tag{13}$$

- The criterion given in [21] for the onset of an explosive oscillatory growth, which again compares the onset of nonlinearity and linear damping

$$\omega_{Be}^2(0) \geqslant \frac{|\gamma_L|^{5/2}}{\gamma_e^{1/2}} \qquad \text{when } \gamma_L < 0. \tag{14}$$

To the accuracy considered here, the first and third criteria cannot be distinguished. Whereas the second condition (whose validity limit simply appears on graph (*d*)) does not seem to be the limiting one (for our set of simulations), the other two are in fair agreement with the mode onset. This suggests that the access to the nonlinear regimes is a major limiting factor for the existence of metastable modes.
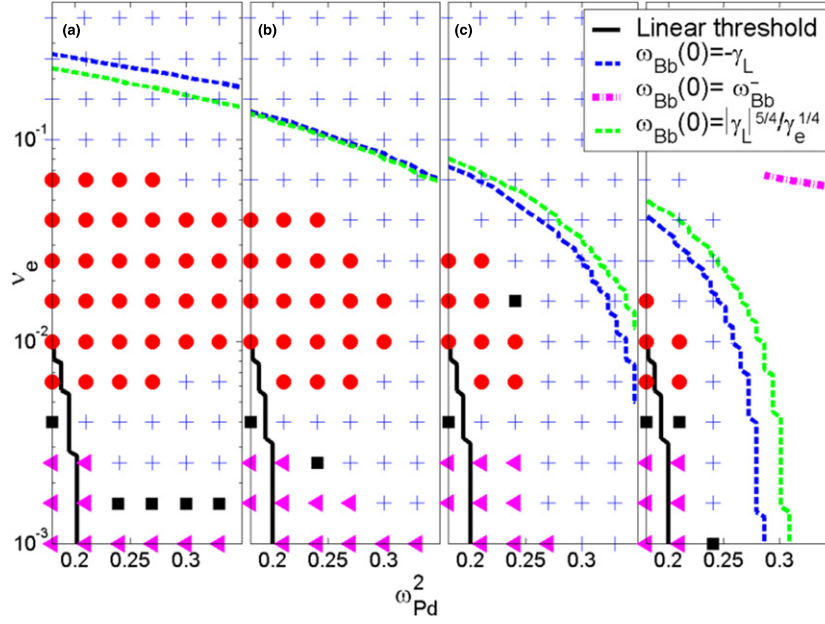
Figure 5. Stability diagrams corresponding to $m_d/m_l = 0.5$, $\nu_d = 0.005$, obtained for various choices of the initial perturbation: (*a*) $\omega_{Bb}(0) = 0.2$; (*b*) $\omega_{Bb}(0) = 0.1$; (*c*) $\omega_{Bb}(0) = 0.05$; (*d*) $\omega_{Bb}(0) = 0.025$.

4. Relevance to real tokamak conditions

We now want to discuss the relevance of the results depicted in the previous paragraphs to realistic tokamak modes, called beta Alfvén eigenmodes (BAEs), which are thought to be driven by fast ions and damped by thermal ion Landau damping [16].

4.1. Relevance of the 1D bump-on-tail model

It is traditional to write Poisson equation in a variational form similar to [26]. Indeed, quasi-neutral low frequency Maxwell equations being linear are equivalent to the extremalization of the electromagnetic Lagrangian

$$\mathcal{L}_\omega = \int d^3x \left(\epsilon_0 |\boldsymbol{E}_\omega|^2 - \frac{|\boldsymbol{B}_\omega|^2}{\mu_0} \right) - \sum_s \int d^3x \, d^3v e_s (\boldsymbol{j}_{s\omega} \cdot \boldsymbol{A}_{s\omega}^* - \rho_{s\omega}\phi_\omega^*)$$

$$= \int d^3x \left(\epsilon_0 |\boldsymbol{E}_\omega|^2 - \frac{|\boldsymbol{B}_\omega|^2}{\mu_0} \right) - \sum_s \int d^3x \, d^3v e_s F_{s\omega} h_{s\omega}^* \qquad (15)$$

by $(\phi_\omega^*, \boldsymbol{A}_\omega^*)$ for any frequency ω, where the ω index can be understood as the use of a Fourier transform. Here, the contribution of all populations of particles is summed over the species s, F_s is the species s distribution function, h_s the hamiltonian acting on the particle population, which fully determines the Vlasov part of the particle response (the left-hand side of equation (1)). Hence, the 1D (or 2D in 6D phase space) bump-on-tail problem can be put in a form which does not depend on its electrostatic character and the resonant nonlinear mechanism considered above has been shown to depend only on the structure of this formulation [21].

9

Consequently, the equivalence between the bump-on-tail and beta Alfvén eigenmode models for the physics at stake only requires to write the particle response in a 2D phase space. In general, a tokamak pertubation involving only one single resonance (one single triplet n in the equation below) can be written in the action-angle variables (α, J) [27] using a hamiltonian of the form [21]

$$H = H_{eq}(J) + h(J, t) \cos\left(n \cdot \alpha - \omega_{r0}t - \int dt \delta\omega_r(t)\right), \tag{16}$$

with $\omega_r = \omega_{r0} + \delta\omega_r(t)$ the instantaneous frequency and ω_{r0} the linear eigenmode frequency, H_{eq} and h, respectively, the equilibrium and perturbed hamiltonian. In the linear regime, resonance occurs for particles verifying $\omega_{r0} = n \cdot \Omega(J) \equiv n \cdot \partial_J H_{eq}$. If a perturbative treatment of the form

$$H = H_{eq}(J_R) + \partial_J H_{eq} \cdot \delta J + h(J_R, t) \cos(n \cdot \alpha - \omega_{r0}t - \int dt \delta\omega_r) \tag{17}$$

is possible around a point J_R $(J = J_R + \delta J)$ of the resonant curve, tridimensional geometric difficulties are removed. Indeed, the dynamics described by equation (17) is fully contained in the variables

$$q = n \cdot \alpha - \omega_{r0}t - \int dt \, \delta\omega_r, \tag{18}$$

$$p = n \cdot \partial_J H - \omega_{r0} - \delta\omega_r \approx n \cdot \partial_J H_{eq} \cdot \delta J - \delta\omega_r, \tag{19}$$

which are conjugate variables for the Hamiltonian

$$\mathcal{H} = \tfrac{1}{2}p^2 - \mathsf{C}h(J_R, t) \cos q + \dot{\delta\omega}_r \, q, \tag{20}$$

with $\mathsf{C} = n \cdot \partial_J \Omega_0(J_R) \cdot n$ the Hamiltonian curvature at resonance in the n-direction. q is similar to an angle variable. Besides, noticing that the variations of the action variables $\dot{\delta J} = -h \sin(q)n$ simply occurs in the direction of n (in 3D action phase space) such that $\delta J = \delta J n$, p can be seen as a measure along n in action space.

The hamiltonian (20) is close to an oscillator and describes the bouncing of the particles inside the perturbation structure in phase space. It can be characterized by the deeply trapped bouncing frequency $\omega_B = \sqrt{\mathsf{C}h(J_R)}$ corresponding to the oscillation frequency in the limit $\dot{\delta\omega}_r \to 0, q \to 0$. When applied to the bump-on-tail problem, we easily recover the bouncing frequency used in the previous paragraphs $\omega_B = \sqrt{|e|Ek/m}$.

Finally, under the assumptions that resonance between one given particle species and the mode is well reproduced by one single resonance, that geometry gradients are sufficiently smooth (to allow the expansion of eqaution (17)) and that simple background dissipative phenomena are present (for the collisional particle response), the 3D electromagnetic beta Alfvén eigenmode problem can be reduced to a simpler 1D electrostatic bump-on-tail model.

4.2. Existence of metastable beta Alfvén eigenmodes

The analysis of section 3 essentially shows that metastable modes can be expected when the nonlinear reduction factors ν_e^* exceeds ν_d^*. The purpose of this section is to estimate these factors for BAEs. Nevertheless, one should not forget that the above analysis simply applies for the perturbative steady-state limit. For BAEs, steady-state behaviours are relevant as confirmed by several experimental observations [17, 28]. The perturbative treatment is more debatable. It applies close to marginal stability when the mode is not too strongly damped by thermal ion Landau damping, which occurs when $\omega_{BAE} \gg v_{ti}/qR$, with ω_{BAE} the linear mode frequency, $v_{ti} \equiv \sqrt{T_i/m_i}$ the ion thermal velocity (T_i the thermal ion temperature and m_i their mass), q the safety factor at the mode localization and R the tokamak major radius. Since ω_{BAE}

is usually estimated to be $\omega_{BAE} = (v_{ti}/R)\sqrt{3.5 + 2T_e/T_i} > v_{ti}/qR$, the perturbative treatment makes some sense and it is particularly appropriate in large q-experiments [29] or experiments with cold ions compared with the electron temperature [16].

To calculate ν_e^* and ν_d^*, we make use of the explicit choice of action-angle variables given in the appendix of [30].

Let us first consider resonance with hot ions, referred to with the index $s = $ h. For BAEs, resonance is likely to occur with the drift precession of trapped fast ions for $(n_1 = 0, n_2 = 0, n_3 = n)$ with n with the BAE toroidal mode number [17]. Resonant dynamics consequently occurs in the 2D phase space defined by the variables $(q = n\alpha_3, p = C_h \delta J_h)$ where for trapped particles $\delta J_h = \delta J_3/n = e_h \delta\Psi/n$ (Ψ the magnetic flux potential) is mainly a radial coordinate.

In this reduced phase space, turbulent radial diffusion is likely to be the main dissipative effect entering the nonlinear resonant dynamics. For diffusive dissipation the above theory of resonant nonlinear reduction still applies (apart from a slight modification of the c factor which multiplies the nonlinear reduction factor) [31] and it still makes sense to assess the reduction factor ν_e^*. To calculate the hot particle bounce frequency inside the mode, we assume the mode structure to be close to its linear shape. Thus, the interaction hamiltonian can be obtained from the BAE linear dispersion relation [17] (or the traditional fishbone-like dispersion relation [32] applied to BAEs) as

$$h_h = \left| \int \frac{d\alpha_1}{2\pi} \int \frac{d\alpha_2}{2\pi} \int \frac{d\alpha_3}{2\pi} \left(e_h \frac{\boldsymbol{v}_{dh} \cdot \nabla\phi}{-i\omega} \right) e^{-in_3\alpha_3} \right| \sim e_h\phi. \tag{21}$$

with $\boldsymbol{v}_{dh}$ the hot particle drift velocity. Thus, $\nu_e^* = \nu_h^* = \nu_h/\omega_{Bh}$ can be derived from

$$\omega_{Bh}^2 = C_h h_h \qquad \text{with } C_h \sim \frac{n^2 q}{e_h r B_0} \frac{1}{L_{ph}} \Omega_{h,3}, \qquad \nu_h \sim \frac{1}{2} \frac{D_h}{\omega_{Bh}^2} \frac{(n\Omega_{h,3})^2}{L_{ph}^2} \tag{22}$$

with B_0 the central magnetic field, L_{ph} a typical gradient of the equilibrium fast ion population, D_h the fast particle radial diffusion coefficient, $\Omega_{h,3}$ the drift-precession frequency of fast particles.

Concerning thermal ions ($s = $ i), resonance with passing ions is most relevant and takes the form $\omega = \pm v_\parallel/qR$ with $v_\parallel$ is the particle parallel velocity. Let us consider one of these two resonances (it is possible if the two resonances are well separated in phase space), for example $\omega = v_\parallel/qR_0$. Again resonant dynamics occurs in a 2D space defined by the variables $(q, p = C_i \delta J_i)$, and we want to determine the physical signification of δJ_i. Using the approximate form of action-angle variables for passing particles $J_2 \approx e_i \Phi(\Psi)$, $J_3 = e_i \Psi(J_2) + m_i R v_\parallel$, it can be seen that δJ_i is dominantly in the same direction as $\delta v_\parallel$ in action phase space, with $\delta v_\parallel/v_{ti} = \delta J_i/m_i q R v_{ti}$.

The main dissipative effect occurring in this reduced phase space is expected to be collisional. To compute the hamiltonian magnitude, we again make use of its linear structure. From [33], it can be estimated in the mode inertial region (where Landau damping is most efficient) as

$$h_i = e \left[\frac{1}{2} \left(\frac{\omega q R_0}{v_{ti}} \right)^2 + \frac{T_e}{T_i} \right] \left(\frac{v_{ti}}{R\omega} \right) \rho_i \partial_r \phi. \tag{23}$$

with ρ_i the ion Larmor radius. Finally, $\nu_d^* = \nu_i^*$ can be derived from

$$\omega_{Bi}^2 = \left(\frac{v_{ti}}{qR_0} \right)^2 \frac{h_i}{T_i} \qquad \nu_i \sim \frac{1}{2} \nu_{ii} \frac{v_{ti}^2}{q^2 R_0^2} \frac{1}{\omega_{Bi}^2} \tag{24}$$

with ν_{ii} is the ion–ion collision frequency.

Using orders of magnitude corresponding to the standard Tore-Supra tokamak experiments with ion heating [17], $R = 2.4\,\text{m}$, $R/L_{ph} = 30$, $T_e/T_i = 1.5$ and taking $\xi \sim 1\,\text{mm}$ (the mode MHD displacement), $\rho_i k_r \sim (\rho_i k_\theta)^{1/4}$ and $\rho_i k_\theta \sim 0.001$ the characteristics of the mode structure in its inertial region ((k_r, k_θ) representing the radial and poloidal mode numbers), $\omega_{BAE}/2\pi \sim \sqrt{3.5 + 2T_e/T_i}(v_{ti}/R)/2\pi \sim 5 \times 10^4\,\text{Hz}$, $D_h = 0.1\,\text{m}^2\,\text{s}^{-1}$ and a collision frequency $\nu_{ii} = 600\,\text{Hz}$, it comes

for fast ions: $2\pi/\omega_{Bh} \sim 2 \times 10^{-4}\,\text{s}$, $\qquad \nu_e^* = \nu_h^* = \nu_h/\omega_{Bh} \sim 0.02$,

for thermal ions: $2\pi/\omega_{Bi} \sim 1 \times 10^{-4}\,\text{s}$, $\qquad \nu_d^* = \nu_i^* = \nu_i/\omega_{Bi} \sim 0.02$. $\qquad$ (25)

Finally, it appears that ν_e^* and ν_d^* are of the same order under the standard tokamak conditions, which shows that the nonlinear reduction of damping is absolutely needed for the determination of saturation. Moreover, since these two factors are of the same order, one can expect particular situations where metastable states are possible.

5. Conclusion

In summary, this paper shows the importance of considering a self-consistent damping in assessing the fast particle driven mode stability. In particular, resonant damping is found to make possible the existence of a subcritical activity. Here, it is explained how steady-state metastable modes can take place. A criterion for their existence is given along with a computation of their expected saturation level, which is in agreement with 1D simulations of the bump-on-tail problem. When applied to tokamak realistic acoustic modes, the consideration of a self-consistent damping is found to be of major importance, and it is legitimate to postulate that metastable modes are possible.

Acknowledgments

References

[1] Heidbrink W W 2008 *Phys. Plasmas* **15** 055501
[2] Merle A, Decker J and Garbet X 2010 *USTTF Meeting (Annapolis, USA)*
[3] Macor A *et al* 2009 *Phys. Rev. Lett.* **102** 155005
[4] Guimarães-Filho Z O *et al* 2010 *37th EPS Conf. on Plasma Physics (Dublin, Ireland)*
[5] Sabot R *et al* 2009 *Nucl. Fusion* **49** 085033
[6] Betti R and Freidberg J P 1992 *Phys. Fluids* B **4** 1465–74
[7] Sharapov S E, Borba D, Fasoli A, Kerner W, Eriksson L, Heeter R F, Huysmans G T A and Mantsinen M J 1999 *Nucl. Fusion* **39** 373–88
[8] Heeter R F, Fasoli A F and Sharapov S E 2000 *Phys. Rev. Lett.* **85** 3177–80
[9] Lilley M K, Breizman B N and Sharapov S E 2009 *Phys. Rev. Lett.* **102** 195003
[10] Fu G Y, Park W, Strauss H R, Breslau J, Chen J, Jardin S and Sugiyama L E 2006 *Phys. Plasmas* **13** 052517
[11] Ödblom A, Breizman B N, Sharapov S E, Hender T C and Pastukhov V P 2002 *Phys. Plasmas* **9** 155–66
[12] Berk H L, Breizman B N and Petviashvili N V 1997 *Phys. Lett.* A **234** 213–8

[13] Zonca F, Briguglio S, Chen L, Fogaccia G and Vlad G 2005 *Nucl. Fusion* **45** 477–84
    http://stacks.iop.org/0029-5515/45/477
[14] Berk H L and Breizman B N 1990 *Phys. Fluids* B **2** 2226–34
[15] Zonca F, Chen L and Santoro R A 1996 *Plasma Phys. Control. Fusion* **38** 2011–28
[16] Boswell C J, Berk H L, Borba D N, Johnson T, Pinches S D and Sharapov S E 2006 *Phys. Lett.* A **358** 154–8
[17] Nguyen C *et al* 2009 *Plasma Phys. Control. Fusion* **51** 095002
[18] Nguyen C, Garbet X, Grandgirard V, Lesur M and Lütjens H 2010 *Phys. Rev. Lett.* at press
[19] Vann R G L, Dendy R O, Rowlands G, Arber T D and D'Ambrumenil N 2003 *Phys. Plasmas* **10** 623–30
[20] Lesur M, Idomura Y and Garbet X 2009 *Phys. Plasmas* **16** 092305
[21] Berk H L, Breizman B N, Candy J, Pekker M and Petviashvili N V 1999 *Phys. Plasmas* **6** 3102–13
[22] Berk H L, Boswell C J, Borba D, Figueiredo A C A, Johnson T, Nave M F F, Pinches S D, Sharapov S E and
    EFDA contributors J 2006 *Nucl. Fusion* **46** 888
[23] O'Neil T 1965 *Phys. Fluids* **8** 2255–62
[24] http://www-math.u-strasbg.fr/calvi/spip.php?rubrique23
[25] Berk H L, Breizman B N and Ye H 1992 *Phys. Rev. Lett.* **68** 3563–6
[26] Edery D, Garbet X, Roubin J P and Samain A 1992 *Plasma Phys. Control. Fusion* **34** 1089–112
[27] Kaufman A N 1972 *Phys. Fluids* **15** 1063–9
[28] Lauber P, Brüdgam M, Curran D, Igochine V, Sassenberg K, Günter S, Maraschek M, García-Muñoz M, Hicks N
    and the ASDEX Upgrade Team 2009 *Plasma Phys. Control. Fusion* **51** 124009
[29] Gorelenkov N N, Berk H L, Fredrickson E, Sharapov S E and Jet Efda Contributors 2007 *Phys. Lett.* A **370** 70–7
[30] Garbet X, Dif-Pradalier G, Nguyen C, Sarazin Y, Grandgirard V and Ghendrih P 2009 *Phys. Plasmas* **16** 062503
[31] Breizman B N, Berk H L, Pekker M S, Porcelli F, Stupakov G V and Wong K L 1997 *Phys. Plasmas* **4** 1559–68
[32] Chen L, White R B and Rosenbluth M N 1984 *Phys. Rev. Lett.* **52** 1122–5
[33] Nguyen C, Garbet X and Smolyakov A I 2008 *Phys. Plasmas* **15** 112502